Systematic Design of Pulse Dosing to Eradicate Persister Bacteria

Garima Singh[1], Mehmet A. Orman[1], Jacinta C. Conrad[1], Michael Nikolaou[*]

[1] Chemical and Biomolecular Engineering Department,
University of Houston, Houston, TX, United States

*Corresponding Author:
nikolaou@uh.edu

Keywords: Persister cells, pulse dosing, modeling

Abstract

A small fraction of infectious bacteria use persistence as a strategy to survive exposure to antibiotics. Pulse dosing of antibiotics has long been considered a potentially effective strategy towards eradication of persisters. Recent studies have demonstrated through *in vitro* experiments that it is indeed feasible to achieve such effectiveness. However, systematic design of pulse dosing regimens to treat persisters is currently lacking. Here we rigorously develop a methodology for the systematic design of optimal pulse dosing strategies for rapid eradication of persisters. A key outcome of the theoretical analysis, on which the proposed methodology is based, is that dosing effectiveness depends mainly on the ratio of corresponding pulse durations. Simple formulas for optimal values of this ratio are derived. The proposed methodology is supported by computer simulations and *in vitro* experiments.

1 INTRODUCTION

Persister cells are a small fraction of a bacterial population that survive otherwise lethal doses of antibiotics by staying at a state of slow or no growth. While these cells remain in the state of persistence, they cannot be killed by conventional antibiotics, unless the cells phenotypically switch to the normal cell state and become susceptible to antibiotics again (Balaban *et al.*, 2004). Persisters are enriched in biofilms (Lewis, 2007) and implicated in many chronic infections such as tuberculosis and relapse of infections such as recurrent urinary tract infection or cystic fibrosis (Mulvey, Schilling and Hultgren, 2001; Blango and Mulvey, 2010; Keren *et al.*, 2011; Zhang, Yew and Barer, 2012; Torrey *et al.*, 2016; Meylan, Andrews and Collins, 2018). Unlike antibiotic-resistant mutant cells, persisters are phenotypic variants that survive treatments without acquiring heritable genetic changes (Balaban *et al.*, 2019). However, prolonged persistence creates favorable conditions for the emergence of the mutant cells (Levin-Reisman *et al.*, 2017; Windels *et al.*, 2019).

Although the term *persister* was coined several decades ago (Bigger, 1944), our knowledge of persisters has accelerated only in the last two decades with the advent of new technologies to isolate and study persister cells (Balaban *et al.*, 2004; Keren *et al.*, 2004). In fact, the mechanisms governing persister formation, survival, and resuscitation are diverse and not sufficiently understood (Balaban *et al.*, 2013). Therefore, developing anti-persister therapeutics remains a challenge. Such development can be broadly classified into two categories: (a) developing new anti-persister drugs, and (b) manipulating the dosing regimen of approved antibiotics. The former relies on detailed knowledge about persister mechanisms (formation, survival, and resuscitation). The latter strategy can be based on population dynamics without complete knowledge of molecular mechanisms, rather capitalizing on the back and forth switching of persisters from normal state to persistence and vice-versa. The idea of pulse dosing to kill persisters is as old as the term persister itself (Bigger, 1944). Yet, there are only sporadic studies on pulse dosing, examining *in vitro* efficacy (Sharma *et al.*, 2015; Meyer *et al.*, 2020) and model fitting of experimental data or characterization of effective pulse dosing strategies (de Leenheer and Cogan, 2009; Cooper and Julius, 2011; Cogan *et al.*, 2012; Imran and Smith, 2014; Himeoka and Mitarai, 2019). A remaining challenge is a simple systematic design of an effective pulse dosing regimen, comprising periods of antibiotic administration at high and low concentrations. Indeed, the alternating periods of antibiotic application and removal are critical to the success of pulse dosing strategies (Cogan *et al.*, 2016; Meyer *et al.*, 2020), as use of an inappropriate strategy fails to achieve eradication (Michiels *et al.*, 2016; van den Bergh *et al.*, 2016). Attempts to connect experiments and modelling (Cogan *et al.*, 2016) have underscored the importance of characterizing optimal dosing regimens in a simple quantitative fashion.

The present study aims at addressing this issue. The specific contributions of this study are (a) rigorous theoretical justification that the efficacy of pulse dosing with alternating on/off periods of antibiotic administration depends on the ratio of the corresponding on/off periods rather than on their individual values; (b) explicit formulas for robustly optimal values of this ratio in terms of easily estimated parameters; and (c) experimental validation of the previous

results *in vitro.* In the rest of the paper, we describe our experimental and modeling studies, present our main results, and close with suggestions for future studies. Proofs and details, to the extent that they provide insight, are included in appendices.

2 MATERIALS AND METHODS

2.1 Experimental

2.1.1 Bacterial strain and plasmid

Escherichia coli wild-type (WT) with a pQE-80L plasmid encoding a green fluorescent protein (GFP) was used. These were obtained from Dr. Mark P. Brynildsen of Princeton University.

2.1.2 Media and chemicals

Luria-Bertani (LB) broth was used for all liquid cultures. LB broth was prepared by dissolving its components (10g Tryptone, 10 g Sodium Chloride, 5 g Yeast Extract) in 1 L distilled water and sterilized with an autoclave. Ampicillin (Sigma Aldrich) was used to treat cells at a constant dose of 100 μg/mL. Phosphate Buffered Saline (PBS) was used to wash the cells to remove Ampicillin. LB agar medium was prepared by dissolving 40 g LB agar premix in 1 L DI water and sterilized with an autoclave. LB agar medium was used to enumerate colony forming units (CFUs) of *E. coli* (Keren *et al.*, 2004; Amato, Orman and Brynildsen, 2013; Orman and Brynildsen, 2015)

2.1.3 Constant (control) and pulse dosing experiments

Bacteria were exposed to Ampicillin in two ways: at constant Ampicillin concentration (control) and at pulsed antibiotic concentration of the same amplitude (pulse on/off dosing, Figure 1).

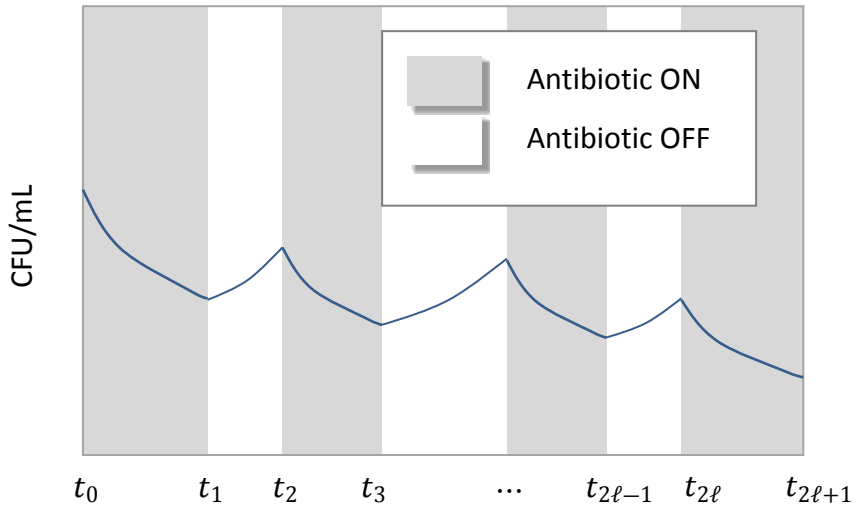

Figure 1. A schematic of the outcome of a pulse dosing regimen showing declining peaks and dips of a bacterial cell population over time.

Each pulse experiment was started by inoculating (1:100-fold) an overnight (24 h) culture of *E. coli* into 25 ml of LB. For selection and retention of plasmids in bacterial cells, 50 μg/ml kanamycin was added in culture media (Orman and Brynildsen, 2015). To induce fluorescent protein expression, 1 mM IPTG was used (Orman and Brynildsen, 2015). The overnight culture was prepared from frozen glycerol stock (-80 ºC). All cells were cultured in a shaker at 37°C and 250 rpm. The pulse dosing schedule was: (a) expose bacteria to Ampicillin (100 μg/ml) for t_{on} h, and (b) wash treated cells and grow in fresh media for t_{off} h. Treated cells were washed with PBS buffer solution to remove the antibiotics. Cells were serially diluted in PBS using 96-well plates, spotted on LB agar, and incubated at 37 °C for 16 h to enumerate CFUs. Bacteria population size was assessed by colony counting on LB-Agar plates.

2.2 Modelling and Simulation

A two-state model (Balaban *et al.*, 2004), comprising two cell-balance differential equations for normal and persister cells, was used in all analysis:

$$\frac{dn}{dt} = K_n n(t) + bp(t) \tag{1}$$

$$\frac{dp}{dt} = an(t) + K_p p(t) \tag{2}$$

or, equivalently,

$$\underbrace{\begin{bmatrix} dn/dt \\ dp/dt \end{bmatrix}}_{d\mathbf{x}/dt} = \underbrace{\begin{bmatrix} K_n & b \\ a & K_p \end{bmatrix}}_{\mathbf{A}} \underbrace{\begin{bmatrix} n(t) \\ p(t) \end{bmatrix}}_{\mathbf{x}(t)} \tag{3}$$

where

$n(t) =$ Number of normal cells at time t

$p(t) =$ Number of persister cells at time t

$\mathbf{x}(t) \stackrel{\text{def}}{=} \begin{bmatrix} n(t) \\ p(t) \end{bmatrix}$

$\mathbf{A} \stackrel{\text{def}}{=} \begin{bmatrix} K_n & b \\ a & K_p \end{bmatrix}$

$a =$ switch rate from normal to persister state

$b =$ switch rate from persister to normal state

$K_n \stackrel{\text{def}}{=} \mu_n - k_n - a =$ net decline / growth rate of normal cells

$K_p \stackrel{\text{def}}{=} \mu_p - k_p - b =$ net decline / growth rate of persister cells

$\mu_n, \mu_p =$ growth rate of normal or persister cells, respectively

$k_n, k_p =$ kill rate of normal or persister cells, respectively

The parameters a, b, K_n, K_p in eqns. (1) and (2) are generally distinct when the antibiotic is administered or not (on/off), resulting in corresponding matrices $\mathbf{A}_{\text{on}}, \mathbf{A}_{\text{off}}$ in eqn. (3). In the constant dosing (control) experiment the antibiotic remained always on, whereas for pulse dosing experiments the antibiotic alternated between on (administered) and off (not administered) with corresponding durations $t_{\text{on}}, t_{\text{off}}$. Therefore, to fit the full data set (at constant and pulse dosing)

by eqns. (1) and (2), parameter estimation generally entailed eight values for estimates of $\{a, b, K_n, K_p\}_{\text{off}}$ and $\{a, b, K_n, K_p\}_{\text{on}}$ during on and off periods, respectively. In addition, because data fit relied on measurements of the total number of cells,

$$c(t) \stackrel{\text{def}}{=} n(t) + p(t) \tag{4}$$

a ninth parameter, namely the initial fraction of persister cells, f_0, was estimated.

Mathematica and MATLAB were used for all modelling, parameter estimation, and analysis computations.

3 RESULTS

We present first a theoretical analysis for characterization of optimal pulse dosing regimens based on the model of eqns. (1) and (2), and subsequently present a series of experiments for validation of analysis results *in vitro*.

3.1 Design of pulse dosing for rapid bacterial population reduction

3.1.1 Characterizing $\{t_{\text{on}}, t_{\text{off}}\}$ *for decline of a bacterial population*

Analysis of eqns. (1) and (2) (APPENDIX A) suggests that successive local peaks of the bacterial population size, $c(t)$, at times $t_{2\ell} \stackrel{\text{def}}{=} \ell(t_{\text{on}} + t_{\text{off}})$, as generally depicted in Figure 1, are characterized as

$$c(t_{2\ell}) = p_1\lambda_1^{\ell} + p_2\lambda_2^{\ell},\ \ \ell = 0, 1, 2, \ldots \tag{5}$$

where λ_1, λ_2 are the eigenvalues of the matrix

$$\mathbf{M} \stackrel{\text{def}}{=} \exp(\mathbf{A}_{\text{off}} t_{\text{off}}) \exp(\mathbf{A}_{\text{on}} t_{\text{on}}) \tag{6}$$

and p_1, p_2 are coefficients depending on the model parameters and initial conditions.

It can be shown (APPENDIX A) that λ_1, λ_2 in eqn. (5) are inside the unit disk. As a result, the pattern of $c(t_{2n})$ in eqn. (5) is downward if and only if the respective on/off periods of pulse dosing, $t_{\text{on}}, t_{\text{off}}$, satisfy the inequality

$$\boxed{\frac{t_{\text{off}}}{t_{\text{on}}} < \left(\frac{t_{\text{off}}}{t_{\text{on}}}\right)_c \stackrel{\text{def}}{=} -\frac{K_{n,\text{on}}}{K_{n,\text{off}}}} \tag{7}$$

Note that the critical value $(t_{\text{off}}/t_{\text{on}})_c$ is positive, because $K_{n,\text{on}} < 0, K_{n,\text{off}} > 0$.

As an example, for the estimates $K_{n,\text{on}}, K_{n,\text{off}}$ shown in Table 1, eqn. (7) yields

$$\frac{t_{\text{off}}}{t_{\text{on}}} < 2.8 \tag{8}$$

for peak-to-peak decline, as shown in Figure 2.

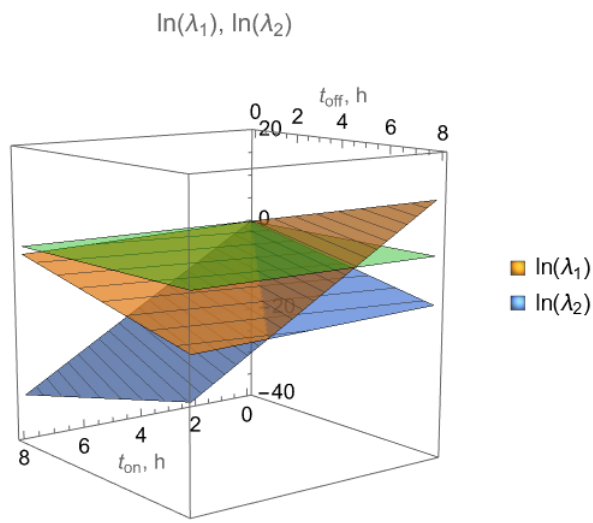

Figure 2. Eigenvalues λ_1,λ_2 of the matrix $\mathbf{M} \stackrel{\text{def}}{=} \exp(\mathbf{A}_{\text{off}} t_{\text{off}}) \exp(\mathbf{A}_{\text{on}} t_{\text{on}})$ governing successive peaks of the bacterial population size, $c(t_{2n})$, under pulse dosing with successive on/off pulses of respective durations $t_{\text{on}}, t_{\text{off}}$, given parameter values in Table 1. Values of $t_{\text{on}}, t_{\text{off}}$ that keep both λ_1,λ_2 below 1 (equivalently $\ln(\lambda_1)$, $\ln(\lambda_2)$ below 0, indicated by the horizontal green plane in the plot) correspond to the green area with a demarcation by a black line of slope $(t_{\text{off}}/t_{\text{on}})_c \approx 2.8$, eqn. (8).

3.1.2 Characterizing $\{t_{\text{on}}, t_{\text{off}}\}$ for rapid peak-to-peak decline of the bacterial population

For pulse dosing with fixed on/off periods t_{on}, t_{off} that satisfy the inequality in eqn. (7), it can be shown (APPENDIX B) that eqn. (3) implies that successive peaks of $c(t)$ at times t_{2n} (Figure 1) decline exponentially over time at a rate,k characterized as

$$\boxed{k \stackrel{\text{def}}{=} \frac{\sqrt{\ln(\lambda_1)\ln(\lambda_2)}}{t_{\text{on}} + t_{\text{off}}} = \frac{\sqrt{(K_{n,\text{off}} x + K_{n,\text{on}})(K_{p,\text{off}} x + K_{p,\text{on}})}}{1 + x}} \tag{9}$$

where

$$x \stackrel{\text{def}}{=} \frac{t_{\text{off}}}{t_{\text{on}}} \tag{10}$$

or, equivalently, with a time constant, $\tau = 1/k$.

It follows immediately (APPENDIX B) that the maximum peak-to-peak decline rate for k (as shown in eqn. (9)) is attained at

$$\boxed{\left(\frac{t_{\text{off}}}{t_{\text{on}}}\right)_{\text{opt}} = \frac{2R_n R_p - R_n - R_p}{2 - R_n - R_p} \approx \frac{R_n}{R_n - 2}} \tag{11}$$

where

$$R_p \stackrel{\text{def}}{=} \frac{K_{p,\text{on}}}{K_{p,\text{off}}}, \quad R_n \stackrel{\text{def}}{=} \frac{K_{n,\text{on}}}{K_{n,\text{off}}} \tag{12}$$

and the approximation in eqn. (11) is based on

$$\frac{K_{p,\text{on}}}{K_{p,\text{off}}} \approx 0 \tag{13}$$

Application of eqn. (11) yields a profile or the optimal ratio $(t_{\text{off}}/t_{\text{on}})_{\text{opt}}$ in terms of the ratios R_p, R_n in eqn. (12) as shown in Figure 3. In that figure, estimates from the experimental data of Figure 2 fitted by parameter estimates in Table 1 are used to mark the indicated point.

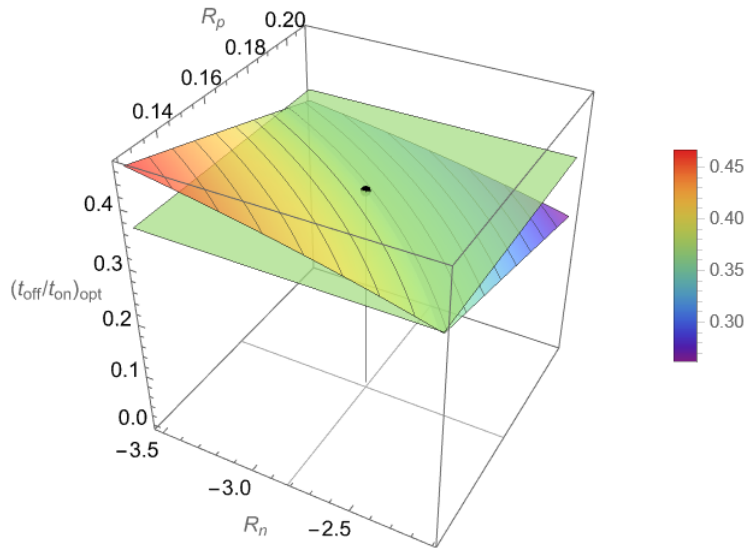

Figure 3. Optimal values of the ratio $t_{\text{on}}/t_{\text{off}}$ that yield maximum decline rate, k, of successive peaks of bacterial population counts, $c(t_{2\ell})$, given values of the ratios R_n, R_p, according to eqn. (11). Values of R_n, R_p are considered in the range $\pm 25\%$ of the experimentally estimated values, which correspond to $(t_{\text{on}}/t_{\text{off}})_{\text{opt}} \approx 0.4$, marked by the black dot and horizontal green plane through it.

To visualize eqns. (7), (9), and (11), estimates of $\{K_n, K_p\}_{\text{off}}$ and $\{K_n, K_p\}_{\text{on}}$ in Table 1 were used to produce a characterization of the peak-to-peak decline rate as a function of t_{on}, t_{off}, as shown in Figure 4.

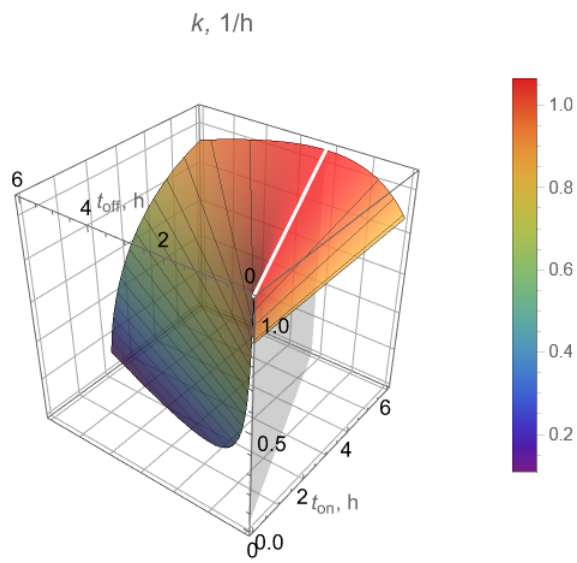

Figure 4. Peak-to-peak decline rate under pulse dosing, k (eqn. (9)) as a function of on/off pulse durations, t_{on},t_{off}, respectively. The decline rate achieves a maximum for $(t_{off}/t_{on})_{opt} \approx 0.4$ according to eqn. (11) (white line) and remains relatively flat for small variations of t_{on}, t_{off}. Note also the straight lines indicating dependence of k on (t_{off}/t_{on})..

A remarkable implication of eqn. (11) is that an optimal ratio t_{off}/t_{on} (in the sense defined in this section) can be approximately assessed by mere knowledge of the ratio $K_{n,on}/K_{n,off}$, which, in turn, can be easily obtained from two simple short-term experiments, namely standard time-growth and time-kill. The corresponding initial slopes in such experiments immediately yield $K_{n,off}$ (time-growth) and $K_{n,on}$ (time-kill), as discussed next. This is a significant simplification of the parameter estimation task for the purpose of pulse dosing regimen design, because it reduces the number of parameters to be estimated from nine (cf. section 2.2) to two. In addition, these two parameters are much easier to estimate than the remaining seven, whose accurate estimates are hard to obtain, as discussed in section 3.3.

3.2 Constant and pulse dosing experiments

Data from a simple time-growth experiment (no antibiotic) and a time-kill experiment (antibiotic at constant concentration) are shown in Figure 5. The slopes from respective curve fits of the data in Figure 5 yield

$$K_{n,off}/\ln(10) \approx 0.5,\ K_{n,on}/\ln(10) = -1.4 \tag{14}$$

(Detailed statistics are provided in APPENDIX C.)

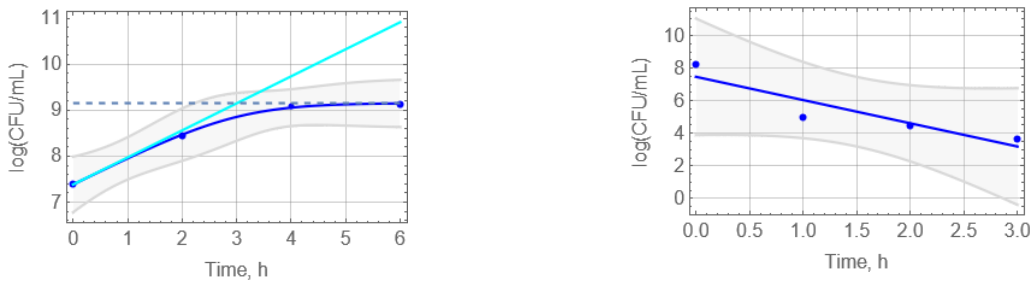

(a) (b)

Figure 5. Time-growth (a) and time-kill (b) experiments for generation of data to assess $t_{\text{on}}/t_{\text{off}}$ for design of pulse dosing. 95%-confidence bands are shown. The slope of the cyan straight line (a) indicates the initial slope of the blue line and corresponds to $K_{n,\text{off}}/\ln(10)$, whereas the blue line slope (b) is $K_{n,\text{on}}/\ln(10)$.

Using the above two estimates for $K_{n,\text{off}}$, $K_{n,\text{on}}$ in eqn. (12) to calculate R_n and substituting the resulting value of R_n into eqn. (11) yields

$$\left(\frac{t_{\text{off}}}{t_{\text{on}}}\right)_{\text{opt}} \approx 0.6 \tag{15}$$

Therefore, to be close to the value of 0.6, pulse dosing with

$$t_{\text{on}} = 3\text{h},\ t_{\text{off}} = 2\text{h} \tag{16}$$

was implemented in validation experiments *in vitro*.

The outcome of pulse dosing using the above t_{on}, t_{off}, along with additional data for continuation of the constant dosing (control) experiment to 13h, are shown in Figure 6. In the case of constant dosing, colonies were seen in all replicates at the end of the 13h treatment $(5 - 100\ \text{CFU/mL})$ whereas in the case of pulse dosing no colony was observed in any replicate in the latter part of the last t_{on} cycle.

3.3 Model parameter estimation with full data set

To confirm that the model used in the analysis for development of the formulas applied in the approach proposed to pulse dosing design, the parameters in eqns. (1) and (2) were fit to the full set of experimental data of Figure 6, with corresponding curves shown in Figure 6 and parameter estimates shown in Table 1.

Table 1 Parameter estimates fitting the experimental data of Figure 6. (standard errors reported)

Parameter	**Antibiotic on**	**Antibiotic off**
K_n	-3.8 ± 0.4	1.35 ± 0.09
K_p	-0.2 ± 0.2	-1.2 ± 0.4
a	0	0
b	0	1.2 ± 0.4
f_0	$9\text{E}-07 \pm 1.6\text{E}-05$	
$\log_{10} c_0$	7.8 ± 0.4	

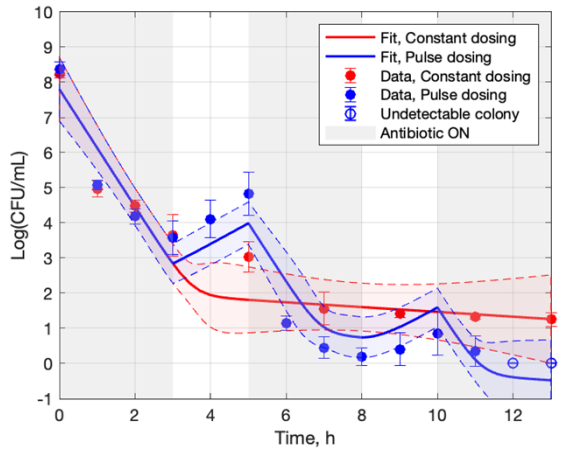

Figure 6. Experimental data and model fit for bacterial population over time, resulting from constant dosing (red) and uniform pulse dosing (blue). The hollow blue circles on the right are set to 0 by convention, to indicate undetectable colony forming units (CFU). 95%-confidence bands are shown.

3.4 Pulse dosing design validation

Eqns. (7) and (8) indicate that bacteria eradication would be achieved if the pulse dosing period ratio $t_{\text{off}}/t_{\text{on}}$ remained below 2.8, based on the short-term data fit (Figure 5), or below 2.4, based on full data fit (Figure 6). This assessment is confirmed via both simulation and experiment.

3.4.1 Simulation

Integration of eqns. (1) and (2) for parameter estimates based on Figure 6 yields the results of Figure 7. That figure shows profiles of the total bacterial population over time for various values of $\{t_{\text{on}}, t_{\text{off}}\}$, anticipated by Figure 4 to correspond to either eradication or growth of the population.

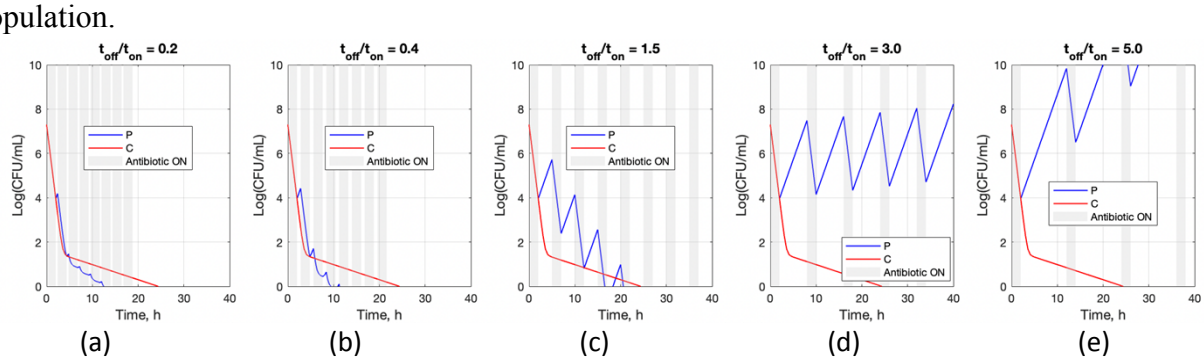

Figure 7. Solution of eqns. (1) and (2) for constant dosing (red) and for uniform pulse dosing (blue) with $t_{\text{on}} = 2\text{h}$ and different values of $t_{\text{off}}/t_{\text{on}}$, given estimates of $\{a, b, K_n, K_p\}_{\text{off}}$ and $\{a, b, K_n, K_p\}_{\text{on}}$ obtained from the experimental data of Figure 6. Outcomes are as anticipated by Figure 4, i.e. eradication at different rates is observed in (a)-(c) and lack of eradication in (d), (e).

3.4.2 Experiment

In addition to the experimental data in Figure 6, example cases of pulse dosing anticipated by the developed theory and by computer simulations not to result in bacterial eradication were also validated through *in vitro* experiments, as shown in Figure 8. This figure shows the outcome (dots) of two pulse dosing experiments corresponding to the same $t_{\text{off}}/t_{\text{on}} = 6$, above the critical value $(t_{\text{off}}/t_{\text{on}})_c = 2.8$ (eqn. (8)). Model predictions (eqns. (1) and (2) with parameter estimates from Table 1 based on data of Figure 6) are also shown.

Note that for $\{t_{\text{on}}, t_{\text{off}}\} = \{3\text{h}, 18\text{h}\}$ the linear model of eqns. (1) and (2) correctly predicts the observed peak-to-peak upward trend, but the model crosses the bacterial population saturation limits (eqn. (A-42)) which are at about 9 $\log(\text{CFU/mL})$ (APPENDIX C) hence the quantitative discrepancy.

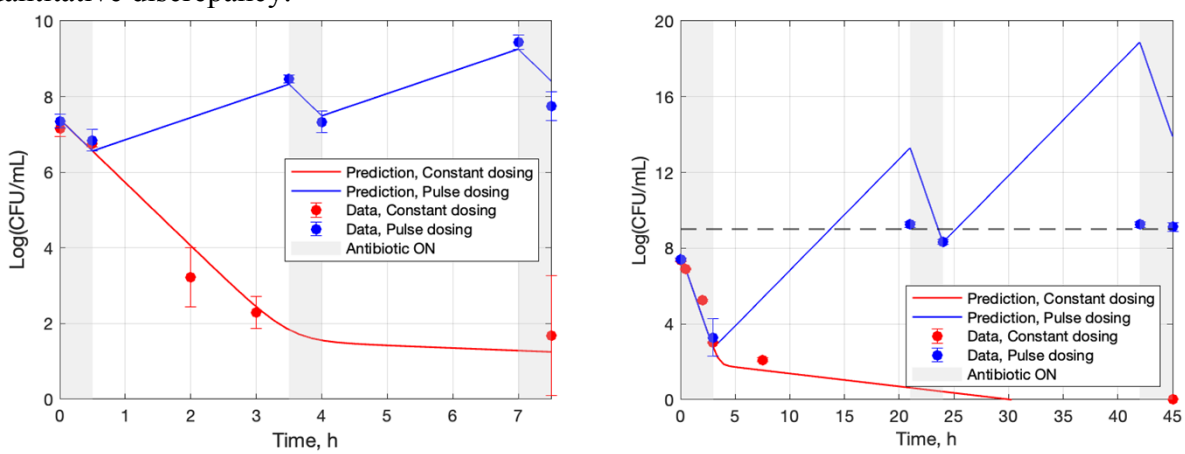

(a) (b)

Figure 8. Experimental (dots) and simulated (lines) values for constant dosing (red) and pulse dosing (blue) with $\{t_{\text{on}}, t_{\text{off}}\} = \{0.5\text{h}, 3\text{h}\}$ (a) and $\{t_{\text{on}}, t_{\text{off}}\} = \{3\text{h}, 18\text{h}\}$ (b) both pulse dosing regimens corresponding to $t_{\text{off}}/t_{\text{on}} = 6 > (t_{\text{off}}/t_{\text{on}})_c$.

Additional experiments were also conducted to test the robustness of pulse dosing in case of non-uniform perturbations of t_{on} around 3h and t_{off} around 2h. The results, shown in Figure 9, suggest rapid bacterial eradication (within about 10h), on par with uniform pulse dosing (cf. results shown in Figure 6 and Figure 7).

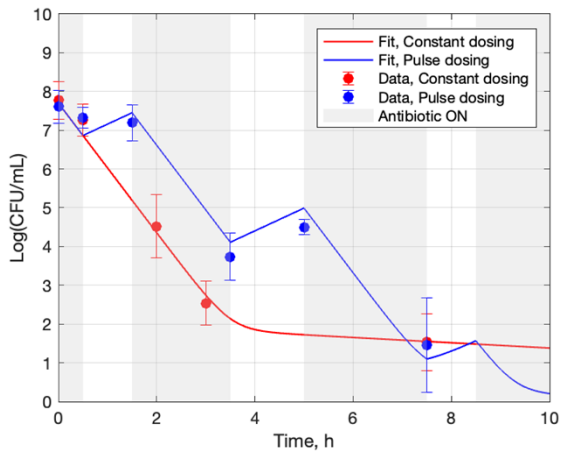

Figure 9. Outcome of non-uniform pulse dosing (and control) for non-uniform perturbations of pulse durations around their nominal values $t_{\text{on}} = 3\text{h}, t_{\text{off}} = 2\text{h}$.

4 Discussion

4.1 Design of pulse dosing for rapid bacterial population reduction

4.1.1 Characterizing $\{t_{\text{on}}, t_{\text{off}}\}$ for decline of a bacterial population

The analysis presented relies on the linear model of eqns. (1) and (2). That model is clearly not valid when the bacterial population reaches its saturation limits after long growth periods (e.g. Figure 5 (a) and eqn. (A-42) in APPENDIX C). Therefore, eqn. (7), which places an upper bound on the ratio $t_{\text{on}}/t_{\text{off}}$ of pulse dosing, is understood to hold for values of t_{off} that do not drive the bacterial population beyond logarithmic growth to saturation.

4.1.2 Characterizing $\{t_{\text{on}}, t_{\text{off}}\}$ for rapid peak-to-peak decline of the bacterial population

Selection of the geometric average of two decline rate constants,

$$k_1 \stackrel{\text{def}}{=} -\frac{\ln(\lambda_1)}{(t_{\text{on}} + t_{\text{off}})},\ k_2 \stackrel{\text{def}}{=} -\frac{\ln(\lambda_2)}{(t_{\text{on}} + t_{\text{off}})} \tag{17}$$

in eqn. (9), captures well an overall decline rate (Figure 10) when early parts of the decline are important.

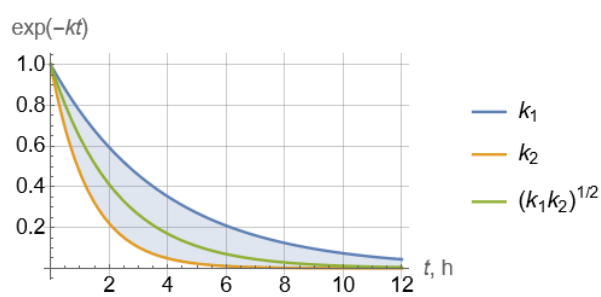

Figure 10. Exponential peak-to-peak decline rate modes corresponding to each individual rate k_1, k_2 (eqn. (17)) and the geometric average rate $k \stackrel{\text{def}}{=} (k_1 k_2)^{1/2}$ (eqn. (9)).

An alternative, focusing more on the long-term decline rate, would be to choose the dominant (smaller) of the two decline rates k_1,k_2 (Figure 10). The results would be somewhat different quantitatively, but of similar nature. This is exemplified in Figure 11, which is the counterpart of Figure 4. Simulations shown in Figure 7 clearly indicate that predictions of peak-to-peak decline rates made by Figure 4 are quantitatively more reliable than those made by Figure 11.

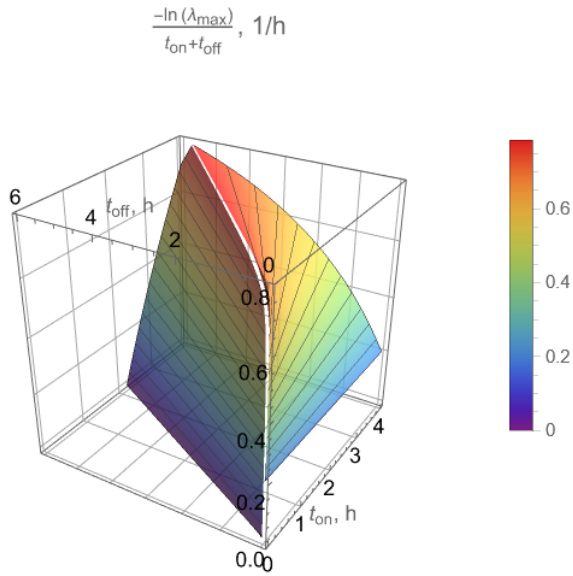

Figure 11. Peak-to-peak actual-time decline rate corresponding to the larger (slower) of the two eigenvalues λ_1, λ_2 of the matrix $\mathbf{M}$ as a function of $t_{\text{on}}, t_{\text{off}}$ for the values of $K_{n,\text{on}}$, $K_{p,\text{on}}$, $K_{n,\text{off}}$, $K_{p,\text{off}}$ in Table 1. The crease line, where the two surfaces intersect, corresponds to eqn. (A-35) and characterizes the highest peak-to-peak actual-time decline rate, for $t_{\text{off}}/t_{\text{on}} = 1.5$.

The quantitative analysis presented in section 3.1 focuses on the rate of peak-to-peak decline, with the intent to design pulse dosing regimens for rapid bacterial eradication. A somewhat more accurate characterization of time to eradication would be provided by focusing on the rate of dip-to-dip decline (c.f. Figure 6 and Figure 7). It can be shown (eqns. (A-20) and (A-21) in APPENDIX A), however, that both peaks and dips of the bacterial population follow the same rate, governed by the eigenvalues λ_1, λ_2 of the matrix $\mathbf{M}$ (eqn. (6)). Because tracking peaks is simpler to analyze than tracking dips, the choice was made to focus on the former, leaving the latter for a future study.

In addition to the quantitative analysis that resulted in the selected values $t_{\text{on}} = 3\text{h}$, $t_{\text{off}} = 2\text{h}$ (eqn. (16)) for the pulse dosing experiment, heuristic analysis was also used to corroborate that choice, as follows:

In the early part of the constant dosing (control) experiment, it is evident (Figure 6) that around 3h persisters start becoming an increasingly significant fraction of the bacterial population (as manifest by the bend in the declining population logarithmic size) and

subsequently dominate the population. Therefore, keeping the antibiotic on beyond 3h would result in reduced killing rate. Furthermore, while turning the antibiotic off starts driving persisters back to normal cells, keeping it off beyond 2h would reach the limits of that drive. While the above analysis suggests that the selected of t_{on}, t_{off} values are sensible, it cannot provide a general characterization of optimal values or establish the importance of the ratio $t_{\text{on}}/t_{\text{off}}$.

Related experiments (Mohiuddin, Kavousi and Orman, 2020) have found that persisters treated for 3h with Ampicillin were able to resuscitate after growth in fresh media for as little as 1h. In our experiments also, a manifold increase in kill rates when treated again with Ampicillin suggested that persisters resuscitated to normal cells indeed within an hour of growth in fresh media.

4.2 Modeling and parameter estimation

Estimation of the four model parameters in eqns. (1) and (2) faces the challenge that measurements of bacterial population size, eqn. (4), are linear combinations of the two solution modes, $q_1\exp(\rho_1 t) + q_2\exp(\rho_2 t)$ (APPENDIX D) with

$$\rho_{1,2} = \frac{1}{2}\left(K_n + K_p \pm \sqrt{4ab + (K_n - K_p)^2}\right) \tag{18}$$

which makes it difficult to estimate all four $\{K_n, K_p, a, b\}$ with good accuracy from data. Nevertheless, assumptions based on fundamental knowledge can facilitate estimation. These assumptions are in accordance with relevant literature (Balaban *et al.*, 2019) and similar observations in our own experiments.

When the antibiotic is on, it follows that $b \approx 0$, because persisters remain dormant, and $a \gtrsim 0$, as some normal cells switch to persisters due to antibiotic stress. Estimation of a nonzero a yielded a very small value, in agreement with the assumption $a \approx 0$.

When there is no antibiotic and cells are grown in fresh media, it follows that $a \approx 0$, as the tendency of normal cells to become dormant is negligible during the early exponential phase (e.g. in less than 3h of growth), whereas $b > 0$, as persisters will be resuscitated shortly (e.g. within an hour) after inoculation in fresh media (Keren et al., 2004; Carvalho et al., 2017a, Mohiuddin, Kavousi and Orman, 2020) . In addition, $K_{p,\text{on}} \approx -b$, because $\mu_{p,\text{on}} \approx 0$ and $k_{p,\text{on}} \approx 0$.

5 Conclusions and Future Work

We have developed a methodology for systematic design of pulse dosing regimens that can eradicate persistent bacteria. The methodology relies on explicit formulas that make use of easily obtainable data from time-growth and time-kill experiments with a bacterial population exposed to antibiotics. Several extensions of this work can be pursued, including:

- Test the outlined strategy on various pairs of pathogenic bacterial strains and antibiotics, including combinations of antibiotics for stubborn infections.
- Extend and test the developed methodology, both theoretically and experimentally, to

353 o Clinically relevant pharmacokinetic profiles of antibiotic administration, e.g.
354 periodic injection followed by exponential decline (Nikolaou *et al.*, 2007);
355 o Reduced antibiotics concentration in consecutive cycles (Imran and Smith, 2014).
356 • The experiments presented used Ampicillin (a β-lactam antibiotic) which is a *time-*
357 *dependent* antibiotic, namely it exhibits best efficacy if administered in periodic
358 injections of as high concentration as possible (Craig and Middleton, 1998). It is worth
359 exploring the performance of the proposed pulse dosing design methodology to
360 *concentration-dependent* antibiotics such as aminoglycosides and quinolones.
361 • Models developed using data from flow cytometry experiments (Mohiuddin, Kavousi and
362 Orman, 2020) can better monitor the heterogeneity of a bacterial population, with
363 potential improvements in modeling and, as a result, pulse dosing design.

364

365

366 *Acknowledgements*
367 The Institute of Allergy and Infectious Diseases of the National Institutes of Health under award
368 number 371 R01AI140287 partially supported the research reported in this publication. The
369 content is solely the responsibility of the authors and does not necessarily represent the official
370 views of the National Institutes of Health. Funding sources had no involvement in study design;
371 in the collection, analysis and interpretation of data, nor in the writing of the report nor in the
372 decision to submit the article for publication.
373 The University of Houston under GEAR grant 2091-H0067-B0421-I113494 (ST 61553)
374 partially supported this study.
375 Michael Nikolaou and Garima Singh gratefully acknowledge substantial help provided by
376 Sayed Golam Mohiuddin to set up and conduct the experimental part of the study.
377

6 APPENDICES

APPENDIX A. Derivation of eqn. (7)

Consider pulse dosing with antibiotic switched on ($C \neq 0$) and off ($C = 0$) at times t_0, t_1, t_2, t_3,... and with respective pulse durations t_{on},t_{off}. Then, eqn. (3) implies

$$\mathbf{x}(t_1) = \exp(\mathbf{A}_{\text{on}} t_{\text{on}})\mathbf{x}(t_0)$$

$$\mathbf{x}(t_2) = \exp(\mathbf{A}_{\text{off}} t_{\text{off}})\mathbf{x}(t_1) = \exp(\mathbf{A}_{\text{off}} t_{\text{off}})\exp(\mathbf{A}_{\text{on}} t_{\text{on}})\mathbf{x}(t_0)$$

$$\mathbf{x}(t_3) = \ldots = \exp(\mathbf{A}_{\text{on}} t_{\text{on}})\exp(\mathbf{A}_{\text{off}} t_{\text{off}})\exp(\mathbf{A}_{\text{on}} t_{\text{on}})\mathbf{x}(t_0)$$

$$\vdots$$

$$\mathbf{x}(t_{2\ell})$$

$$= \underbrace{\left(\overbrace{\exp(\mathbf{A}_{\text{off}} t_{\text{off}})\,\exp(\mathbf{A}_{\text{on}} t_{\text{on}})}^{\mathbf{M}}\right)\ldots\left(\overbrace{\exp(\mathbf{A}_{\text{off}} t_{\text{off}})\,\exp(\mathbf{A}_{\text{on}} t_{\text{on}})}^{\mathbf{M}}\right)}_{\ell}\mathbf{x}(t_0)$$

$$= \mathbf{M}^{\ell}\mathbf{x}(t_0), \quad \ell = 0, 1, 2, \ldots$$

and

$$\mathbf{x}(t_{2\ell+1})$$

$$= \exp(\mathbf{A}_{\text{on}} t_{\text{on}})\underbrace{\left(\overbrace{\exp(\mathbf{A}_{\text{off}} t_{\text{off}})\,\exp(\mathbf{A}_{\text{on}} t_{\text{on}})}^{\mathbf{M}}\right)\ldots\left(\overbrace{\exp(\mathbf{A}_{\text{off}} t_{\text{off}})\,\exp(\mathbf{A}_{\text{on}} t_{\text{on}})}^{\mathbf{M}}\right)}_{\ell}\mathbf{x}(t_0)$$

$$= \exp(\mathbf{A}_{\text{on}} t_{\text{on}})\mathbf{M}^{\ell}(t_0), \quad \ell = 0, 1, 2, \ldots$$

Therefore

$$c(t_{2\ell}) = \mathbf{c}^{\top}\mathbf{M}^{\ell}\mathbf{x}(t_0) \tag{A-20}$$

$$c(t_{2\ell+1}) = \mathbf{c}^{\top}\exp(\mathbf{A}_{\text{on}} t_{\text{on}})\mathbf{M}^{\ell}\mathbf{x}(t_0) \tag{A-21}$$

where $\mathbf{c}^{\top} = [1 \quad 1]$.

The above two equations suggest that peaks and dips of $c(t)$ at times $t_{2\ell}$ and $t_{2\ell+1}$, respectively, increase or decrease at the same rate, governed by the eigenvalues λ_1, λ_2 of the matrix

$$\mathbf{M} \stackrel{\text{def}}{=} \exp(\mathbf{A}_{\text{off}} t_{\text{off}})\exp(\mathbf{A}_{\text{on}} t_{\text{on}}) \tag{A-22}$$

as

$$c(t_{2\ell}) = \mathbf{c}^{\top}\mathbf{M}^{\ell}\mathbf{x}(t_0) = \mathbf{c}^{\top}\mathbf{P}\boldsymbol{\Lambda}^{\ell}\mathbf{P}^{-1}\mathbf{x}(t_0) \tag{A-23}$$

and similarly for $c(t_{2\ell+1})$.

Now, because $a \approx 0$, the eigenvalues, ρ_1, ρ_2 of

$$\mathbf{A} \stackrel{\text{def}}{=} \begin{bmatrix} K_n & b \\ a & K_p \end{bmatrix} \tag{A-24}$$

in eqn. (3) are approximately

$$\boxed{\rho_1 \approx K_n, \ \rho_2 \approx K_p} \tag{A-25}$$

When the antibiotic is on, then $b \approx 0$, and

$$K_{n,\text{on}} < K_{p,\text{on}} < 0 \tag{A-26}$$

with $K_{p,\text{on}}$ closer to 0 than $K_{n,\text{on}}$, because $K_{p,\text{on}}$ refers to persisters, in contrast to $K_{n,\text{on}}$, which refers to normal cells that get killed much faster (e.g. see Table 1). In addition, the corresponding eigenvectors of $\mathbf{A}_{\text{on}}$ are $\mathbf{w}_{1,\text{on}} = [1 \quad 0]^\top$, $\mathbf{w}_{2,\text{on}} = [0 \quad 1]^\top$. Therefore,

$$\exp(\mathbf{A}_{\text{on}} t_{\text{on}}) = \begin{bmatrix} \exp(K_{n,\text{on}} t_{\text{on}}) & 0 \\ 0 & \exp(K_{p,\text{on}} t_{\text{on}}) \end{bmatrix} \tag{A-27}$$

Similarly, when the antibiotic is off, it follows that

$$K_{p,\text{off}} < 0 < K_{n,\text{off}} \tag{A-28}$$

because the normal cell subpopulation grows, whereas persister cells decline due to their returning to the state of normal cells (e.g. see Table 1). In addition, the corresponding eigenvectors of $\mathbf{A}_{\text{off}}$ are $\mathbf{w}_{1,\text{off}} = [1 \quad 0]^\top$, $\mathbf{w}_{2,\text{off}} = [1 \quad \xi]^\top$ where $\xi = (K_p - K_n)/b$. Therefore

$$\exp(\mathbf{A}_{\text{off}} t_{\text{off}}) = \exp(K_{n,\text{off}} t_{\text{off}}) \mathbf{w}_{1,\text{off}} \mathbf{z}_{1,\text{off}}^\top + \exp(K_{p,\text{off}} t_{\text{off}}) \mathbf{w}_{2,\text{off}} \mathbf{z}_{2,\text{off}}^\top \tag{A-29}$$

where $\mathbf{z}_{1,\text{off}}^\top = [1 \quad -1/\xi]$, $\mathbf{z}_{2,\text{off}}^\top = [1 \quad 1/\xi]$ are the rows of the inverse modal matrix.

Combination of the last two equations (A-29) and (A-27) with the above definition of $\mathbf{M}$ in eqn. (A-22) yields

$$\mathbf{M} = \begin{bmatrix} \exp(K_{n,\text{off}} t_{\text{off}} + K_{n,\text{on}} t_{\text{on}}) & X \\ 0 & \exp(K_{p,\text{off}} t_{\text{off}} + K_{p,\text{on}} t_{\text{on}}) \end{bmatrix} \tag{A-30}$$

where the actual form of X in the above eqn. (A-30) does not affect the eigenvalues of $\mathbf{M}$, which are

$$\boxed{\lambda_1 = \exp(K_{n,\text{off}} t_{\text{off}} + K_{n,\text{on}} t_{\text{on}}), \ \lambda_2 = \exp(K_{p,\text{off}} t_{\text{off}} + K_{p,\text{on}} t_{\text{on}})} \tag{A-31}$$

For $\mathbf{M}^\ell$ to decline as ℓ increases, it is necessary and sufficient that both $0 < \lambda_1 < 1$ and $0 < \lambda_2 < 1$, which is equivalent to

$$K_{n,\text{off}} t_{\text{off}} + K_{n,\text{on}} t_{\text{on}} < 0 \Leftrightarrow \boxed{\frac{t_{\text{off}}}{t_{\text{on}}} < -\frac{K_{n,\text{on}}}{K_{n,\text{off}}}} \tag{A-32}$$

and

$$K_{p,\text{off}} t_{\text{off}} + K_{p,\text{on}} t_{\text{on}} < 0 \Leftrightarrow \frac{t_{\text{off}}}{t_{\text{on}}} > -\frac{K_{p,\text{on}}}{K_{p,\text{off}}} \tag{A-33}$$

in view of the inequalities in eqns. (A-26) and (A-28).

The inequality in eqn. (A-33) is trivially satisfied, because $\frac{t_{\text{off}}}{t_{\text{on}}} > 0$ and $-\frac{K_{p,\text{on}}}{K_{p,\text{off}}} < 0$. Therefore, it is the inequality in eqn. (A-32) that characterizes the feasible region for $t_{\text{off}}/t_{\text{on}}$.

APPENDIX B. Optimal rate of decline for bacterial population peaks characterized by eqn. (9)

Eqn. (A-23) implies that successive peaks of $c(t)$ at times $t_{2\ell}$ (Figure 1) are characterized as

$$c(t_{2\ell}) = p_1\lambda_1^{\ell} + p_2\lambda_2^{\ell},\ \ \ell = 0, 1, 2, \ldots \tag{A-34}$$

where λ_1, λ_2 are the eigenvalues of $\mathbf{M}$ and p_1, p_2 are coefficients depending on the model parameters and initial conditions. Each of the two terms $\lambda_1^{\ell},\ \lambda_2^{\ell}$ in eqn. (A-34) corresponds to a decline ratio from time point $t_{2\ell}$ to $t_{2(\ell+1)}$. For values of $t_{\text{off}}/t_{\text{on}}$ satisfying eqn. (A-32), which guarantees $0 < \lambda_1 < 1,\ 0 < \lambda_2 < 1$ hence decline of successive peaks, the larger of λ_1, λ_2 captures the slower of the two modes of decline ratio from peak to peak. The two planes characterized by the inequalities in eqns. (A-32) and (A-33) written as equalities (cf. Figure 2) intersect at the straight line $\lambda_1 = \lambda_2$ which yields

$$\boxed{\frac{t_{\text{off}}}{t_{\text{on}}} = \frac{K_{p,\text{on}} - K_{n,\text{on}}}{K_{n,\text{off}} - K_{p,\text{off}}} > 0} \tag{A-35}$$

as exemplified in Figure 12 for the parameter values in Table 1.

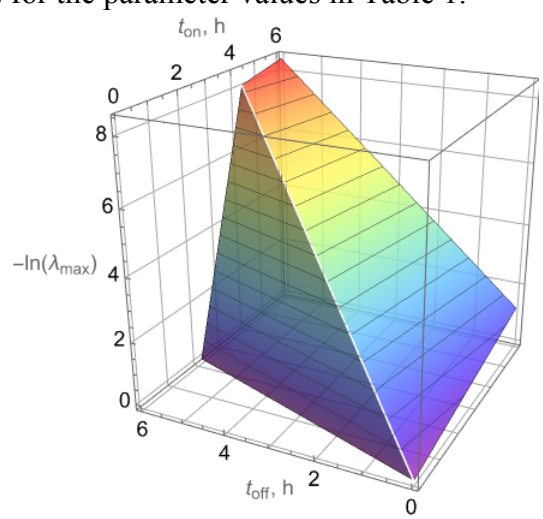

Figure 12. Larger (slower) of the two eigenvalues λ_1, λ_2 of the matrix $\mathbf{M}$ as a function of $t_{\text{on}}, t_{\text{off}}$ for the values of $K_{n,\text{on}}$, $K_{p,\text{on}}$, $K_{n,\text{off}}$, $K_{p,\text{off}}$ in Table 1. The crease line where the two planes intersect corresponds to eqn. (A-35) and characterizes the highest peak-to-peak decline ratio at discrete time points $t_{2\ell} \stackrel{\text{def}}{=} \ell(t_{\text{on}}, + t_{\text{off}})$.

The peak-to-peak decline ratio for each mode at discrete time points $t_{2\ell} \stackrel{\text{def}}{=} \ell(t_{\text{on}}, + t_{\text{off}})$ can be easily converted to actual time rate:

$$\lambda^{\ell} = \exp\left(\ell \ln(\lambda)\right) = \exp\left(\frac{t_{2\ell}}{t_{\text{on}} + t_{\text{off}}} \ln(\lambda)\right) \tag{A-36}$$

which, combined with eqn. (A-31) immediately implies actual-time decline rates

$$k_1 = \frac{\ln(\lambda_1)}{t_{\text{on}} + t_{\text{off}}} = \frac{K_{n,\text{off}}t_{\text{off}} + K_{n,\text{on}}t_{\text{on}}}{t_{\text{on}} + t_{\text{off}}},\ \ k_2 = \frac{\ln(\lambda_2)}{t_{\text{on}} + t_{\text{off}}} = \frac{K_{p,\text{off}}t_{\text{off}} + K_{p,\text{on}}t_{\text{on}}}{t_{\text{on}} + t_{\text{off}}} \tag{A-37}$$

or corresponding time constant

$$\tau_1 = \frac{1}{k_1},\ \ \tau_2 = \frac{1}{k_2} \tag{A-38}$$

as indicated in Figure 11.

Note that the values of k_1,k_2 or τ_1, τ_2 depend on the ratio $\frac{t_{\text{off}}}{t_{\text{on}}}$ rather than on individual values of t_{on}, t_{off}.

To capture with a single term both modes of peak-to-peak decline corresponding to λ_1, λ_2 in eqn. (A-34), one can use the geometric average of k_1, k_2 from eqn. (A-37), i.e.

$$k \stackrel{\text{def}}{=} \sqrt{k_1 k_2} = \frac{\sqrt{\ln(\lambda_1)\ln(\lambda_2)}}{t_{\text{on}} + t_{\text{off}}} = \frac{\sqrt{(K_{n,\text{off}} t_{\text{off}} + K_{n,\text{on}} t_{\text{on}})(K_{p,\text{off}} t_{\text{off}} + K_{p,\text{on}} t_{\text{on}})}}{t_{\text{on}} + t_{\text{off}}} \tag{A-39}$$

or, equivalently the geometric average of τ_1, τ_2 from eqn. (A-38), both of which yield eqn. (9).

To characterize the maximum of the overall decline rate in eqn. (A-39), first observe that

$$k = \frac{\sqrt{(K_{n,\text{off}} x + K_{n,\text{on}})(K_{p,\text{off}} x + K_{p,\text{on}})}}{1 + x} \tag{A-40}$$

where $x \stackrel{\text{def}}{=} \frac{t_{\text{off}}}{t_{\text{on}}}$. Then the setting $dk/dx = 0$ immediately yields

$$\left(\frac{t_{\text{off}}}{t_{\text{on}}}\right)_{\text{opt}} = \frac{2K_{n,\text{on}}K_{p,\text{on}} - K_{n,\text{on}}K_{p,\text{off}} - K_{n,\text{off}}K_{p,\text{on}}}{2K_{n,\text{off}}K_{p,\text{off}} - K_{n,\text{on}}K_{p,\text{off}} - K_{n,\text{off}}K_{p,\text{on}}} \tag{A-41}$$

which is eqn. (11).

APPENDIX C. Estimation of $K_{n,\mathrm{off}}$, $K_{n,\mathrm{on}}$ from data in Figure 5

Assuming that persister cells are initially a tiny minority in the time-growth experiment (antibiotic off), the standard cell-balance equation is

$$\frac{dc}{dt} = K_{n,\mathrm{off}} c(t)\left(1 - \frac{c(t)}{c_{\max}}\right) \Leftrightarrow c(t) = c_0 \exp(K_{n,\mathrm{off}} t) \frac{1}{1 + \frac{c_0}{c_{\max}}(\exp(K_{n,\mathrm{off}} t) - 1)} \tag{A-42}$$

Application to the data shown in Figure 5 (left) yields

	Estimate	Standard Error
$K_{n,\mathrm{off}}$	1.35	0.09
c_0	2.4×10^7	0.3×10^7
$c_{\max}$	1.4×10^9	0.1×10^9

In the time-kill experiment, eqn. (A-42) written for a declining population before persister cells take over becomes

$$\frac{dc}{dt} = K_{n,\mathrm{on}} c(t) \Leftrightarrow c(t) = c_0 \exp(K_{n,\mathrm{on}} t) \tag{A-43}$$

Application to the data shown in Figure 5 (right) yields

	Estimate	Standard Error
$K_{n,\mathrm{on}}$	-3.3	1.0
$\log_{10} c_0$	7.5	0.8

APPENDIX D. Analytical solution of the eqns. (1) and (2)

Given the eigenvalues

$$\rho_{1,2} = \frac{K_n + K_p}{2} \pm \frac{\sqrt{4ab + (K_n - K_p)^2}}{2}$$

of the matrix **A**, yields

$$c(t) = e^{\rho_1 t}\underbrace{\left(\frac{n_0 + p_0}{2} + \frac{(K_n - K_p)(n_0 - p_0)/2 + an_0 + bp_0}{\sqrt{4ab + (K_n - K_p)^2}}\right)}_{q_1}$$

$$+ e^{\rho_2 t}\underbrace{\left(\frac{n_0 + p_0}{2} - \frac{(K_n - K_p)(n_0 - p_0)/2 + an_0 + bp_0}{\sqrt{4ab + (K_n - K_p)^2}}\right)}_{q_2}$$

7 REFERENCES

Amato, S.M., Orman, M.A. and Brynildsen, M.P. (2013) "Metabolic Control of Persister Formation in Escherichia coli," *Molecular Cell* [Preprint]. doi:10.1016/j.molcel.2013.04.002.

Balaban, N.Q. *et al.* (2004) "Bacterial persistence as a phenotypic switch," *Science*, 305(5690), pp. 1622–1625. doi:10.1126/science.1099390.

Balaban, N.Q. *et al.* (2013) "A problem of persistence: Still more questions than answers?," *Nature Reviews Microbiology*, pp. 587–591. doi:10.1038/nrmicro3076.

Balaban, N.Q. *et al.* (2019) "Definitions and guidelines for research on antibiotic persistence," *Nature Reviews Microbiology*, 17(7), pp. 441–448. doi:10.1038/s41579-019-0196-3.

van den Bergh, B. *et al.* (2016) "Frequency of antibiotic application drives rapid evolutionary adaptation of Escherichia coli persistence," *Nature Microbiology*, 1(5). doi:10.1038/nmicrobiol.2016.20.

Bigger, J.W. (1944) "Treatment of Staphylococcal Infections With Penicillin By Intermittent Sterilisation," *The Lancet*, 244(6320), pp. 497–500. doi:10.1016/S0140-6736(00)74210-3.

Blango, M.G. and Mulvey, M.A. (2010) "Persistence of uropathogenic Escherichia coli in the face of multiple antibiotics," *Antimicrobial Agents and Chemotherapy*, 54(5), pp. 1855–1863. doi:10.1128/AAC.00014-10.

Cogan, N.G. *et al.* (2012) "Optimal control strategies for disinfection of bacterial populations with persister and susceptible dynamics," *Antimicrobial Agents and Chemotherapy*, 56(9), pp. 4816–4826. doi:10.1128/AAC.00675-12.

Cogan, N.G. *et al.* (2016) "Theoretical and experimental evidence for eliminating persister bacteria by manipulating killing timing," *FEMS Microbiology Letters*, 363(23), pp. 1–6. doi:10.1093/femsle/fnw264.

Cooper, N.G. and Julius, A.A. (2011) "Bacterial persistence: Mathematical modeling and optimal treatment strategy," in *Proceedings of the American Control Conference*. Institute of Electrical and Electronics Engineers Inc., pp. 3502–3507. doi:10.1109/acc.2011.5991194.

Craig, W.A. and Middleton, W.S. (1998) *Pharmacokinetic/Pharmacodynamic Parameters: Rationale for Antibacterial Dosing of Mice and Men*, *Clinical Infectious Diseases*. Available at: https://academic.oup.com/cid/article/26/1/1/350424.

Himeoka, Y. and Mitarai, N. (2019) "When to wake up? The optimal waking-up strategies for starvation-induced persistence." Available at: http://arxiv.org/abs/1912.12682.

Imran, M. and Smith, H. (2014) "A model of optimal dosing of antibiotic treatment in biofilm," *Mathematical Biosciences and Engineering*, 11(3), pp. 547–571. doi:10.3934/mbe.2014.11.547.

Keren, I. *et al.* (2004) "Persister cells and tolerance to antimicrobials," *FEMS Microbiology Letters*, 230(1), pp. 13–18. doi:10.1016/S0378-1097(03)00856-5.

Keren, I. *et al.* (2011) "Characterization and Transcriptome Analysis of Mycobacterium tuberculosis Persisters." doi:10.1128/mBio.00100-11.

de Leenheer, P. and Cogan, N.G. (2009) "Failure of antibiotic treatment in microbial populations," *Journal of Mathematical Biology*, 59(4), pp. 563–579. doi:10.1007/s00285-008-0243-6.

Levin-Reisman, I. *et al.* (2017) "Antibiotic tolerance facilitates the evolution of resistance," *Science*, 355(6327), pp. 826–830. doi:10.1126/science.aaj2191.

Lewis, K. (2007) "Persister cells, dormancy and infectious disease," *Nature Reviews Microbiology*, 5(1), pp. 48–56. doi:10.1038/nrmicro1557.

Meyer, K.J. *et al.* (2020) "Pulse Dosing of Antibiotic Enhances Killing of a Staphylococcus aureus Biofilm," *Frontiers in Microbiology*, 11. doi:10.3389/fmicb.2020.596227.

Meylan, S., Andrews, I.W. and Collins, J.J. (2018) "Targeting Antibiotic Tolerance, Pathogen by Pathogen," *Cell* [Preprint]. doi:10.1016/j.cell.2018.01.037.

Michiels, J.E. *et al.* (2016) "In vitro emergence of high persistence upon periodic aminoglycoside challenge in the ESKAPE pathogens," *Antimicrobial Agents and Chemotherapy*, 60(8), pp. 4630–4637. doi:10.1128/AAC.00757-16.

Mohiuddin, S.G., Kavousi, P. and Orman, M.A. (2020) "Flow-cytometry analysis reveals persister resuscitation characteristics," *BMC Microbiology*, 20(1). doi:10.1186/s12866-020-01888-3.

Mulvey, M.A., Schilling, J.D. and Hultgren, S.J. (2001) "Establishment of a persistent Escherichia coli reservoir during the acute phase of a bladder infection," *Infection and Immunity*, 69(7), pp. 4572–4579. doi:10.1128/IAI.69.7.4572-4579.2001.

Nikolaou, M. *et al.* (2007) "Modeling of microbial population responses to time-periodic concentrations of antimicrobial agents," *Annals of Biomedical Engineering*, 35(8). doi:10.1007/s10439-007-9306-x.

Orman, M.A. and Brynildsen, M.P. (2015) "Inhibition of stationary phase respiration impairs persister formation in E. coli," *Nature Communications*, 6. doi:10.1038/ncomms8983.

Sharma, B. *et al.* (2015) "Borrelia burgdorferi, the Causative Agent of Lyme Disease, Forms Drug-Tolerant Persister Cells." doi:10.1128/AAC.00864-15.

Torrey, H.L. *et al.* (2016) "High persister mutants in mycobacterium tuberculosis," *PLoS ONE*, 11(5), pp. 1–28. doi:10.1371/journal.pone.0155127.

Windels, E.M. *et al.* (2019) "Bacterial persistence promotes the evolution of antibiotic resistance by increasing survival and mutation rates," *The ISME Journal*, 13(5), pp. 1239–1251. doi:10.1038/s41396-019-0344-9.

Zhang, Y., Yew, W.W. and Barer, M.R. (2012) "Targeting Persisters for Tuberculosis Control," *Antimicrobial Agents and Chemotherapy*, 56(5), pp. 2223 LP – 2230. doi:10.1128/AAC.06288-11.